

REGINA JEZIÓRSKA, BARBARA ŚWIERZ-MOTYSIA, AGNIESZKA SZADKOWSKA, BOGDAN MARCINIEC*, HIERONIM MACIEJEWSKI*, MICHAŁ DUTKIEWICZ*, IRENA LESZCZYŃSKA

Industrial Chemistry Research Institute, Rydygiera 8, 01-793 Warszawa, Poland

*Adam Mickiewicz University, Poznan, Poland

e-mail: regina.jeziorska@ichp.pl

Effect of POSS on morphology, thermal and mechanical properties of polyamide 6

Summary — Polyamide nanocomposites with different octakis(dimethylsiloxy, 3-glycidoxypropyl)octasilsesquioxanes (POSS) contents (0.5, 2, 4 wt. %) were obtained during melt blending. SEM results showed that POSS are uniformly dispersed in polyamide 6 matrix (Fig. 1). FT-IR and DSC analysis indicated that the addition of POSS promotes modifications of the polyamide crystal structure, which consist of the progressive development of α crystals and significant increase in the glass transition temperature, crystallization temperature and the crystallization rate of the polyamide 6 (Figs. 2 and 3, Tab. 1). Tensile tests, performed on dried samples, revealed that strength and elongation at break were appreciably modified by the presence of POSS (Fig. 4, Tab. 2). Compared with the neat polyamide 6, the impact strength of PA 6/POSS composites is enhanced (Tab. 2). Dynamic mechanical thermal analysis (DMTA) demonstrated that both the storage modulus (G') and relaxation temperatures (T_{α} , T_{β} and T_{γ}), especially glass transition temperature (T_{α}) of the PA6/POSS composites significantly increased (Fig. 5, Tab. 3).

Keywords: polyamide 6, POSS, nanocomposites, dispersion, mechanical properties, thermo-mechanical properties.

WPLYW POSS NA STRUKTURĘ, WŁAŚCIWOŚCI CIEPLNE I MECHANICZNE POLIAMIDU 6

Streszczenie — Nanokompozyty poliamidu 6 z różną zawartością oktakis(dimetylosiloksy, 3-glicydoksypropylo)oktasilseskwioksanu (0,5; 2; 4 % mas.) otrzymano w procesie przetwórstwa. Mikrofotografie SEM wykazały równomierny stopień zdyspergowania POSS w osnowie poliamidu 6 (rys. 1). Za pomocą metod FT-IR i DSC stwierdzono, że dodatek POSS modyfikuje strukturę krystaliczną poliamidu, w wyniku utworzenia fazy krystalicznej α następuje istotny wzrost temperatury zeszklenia i krystalizacji oraz szybkości krystalizacji poliamidu 6 (rys. 2 i 3, tab. 1). Ocena właściwości mechanicznych nanokompozytu (wysuszonych próbek) wykazała istotny wpływ POSS na naprężenie i wydłużenie względne przy zerwaniu PA 6/POSS oraz wyraźny wzrost udarności w porównaniu z właściwościami czystego poliamidu (rys. 4, tab. 2). Za pomocą dynamicznej analizy termomechanicznej (DMTA) kompozytów PA 6/POSS stwierdzono znaczący wzrost modułu zachowawczego (G') i temperatury przejść relaksacyjnych (T_{α} , T_{β} and T_{γ}), a w szczególności temperatury zeszklenia (T_{α}) (rys. 5, tab. 3).

Słowa kluczowe: poliamid 6, POSS, nanokompozyty, dyspersja, właściwości mechaniczne, właściwości termomechaniczne.

INTRODUCTION

Polyhedral oligomeric silsesquioxane (POSS) is three-dimensional structurally well defined cage-like molecule represented by the general formula $(RSiO_{1.5})_n$, where R is a hydrogen or an organic group, such as alkyl, aryl or any of their derivatives at the corners of the cage and $n = 6, 8, 10$ or higher [1]. A variety of reactive and non-reactive functional groups can be introduced into their molecule so that POSS chemistry becomes very flexible [2]. Several polymeric systems have been taken into

account incorporating POSS cages both in thermoplastics matrices, such as polyolefins, polyamides, polyesters, and in thermosets, mainly epoxy resins [3–8].

Polymer/inorganic nanocomposites prepared via melt compounding have become a popular topic in material science because of their markedly improved properties and relatively facile preparation procedures [9–11]. Indeed, nanocomposites have been formed using a variety of shear devices (*e.g.* extruders, mixers, ultrasonicators, *etc.*). Of these melt processing techniques, twin screw extrusion has proven to be most effective for the dispersion

of nanoparticles [12–14]. Enhanced characteristics in such composites have so far been reported as a synergistic contribution resulting from the effective combination of nanoparticles and a polymer matrix. However, whether nanoparticles are able to bring positive effects into play depends on their dispersibility in the matrix. Because of high surface energy, these particles have a great inclination for agglomeration, especially in polymer melts that are characterized by high viscosity. Therefore, the preparation of nanocomposites with uniformly distributed nanoparticles is a challenge [15, 16]. Recent studies have demonstrated that melt processing conditions play a key role in achieving high levels of dispersion. Results from these studies indicate that an optimum balance between residence time and level of shear is required to facilitate the dispersion of nanoparticles. In addition, proper choice of nanoparticles chemistry is critical [17–19].

In this paper, the preliminary study on the effect of octakis(dimethylsiloxy, 3-glycidoxypropyl)octasilsesquioxanes (POSS) content on the morphology, thermal and mechanical properties of polyamide 6 (PA6) nanocomposites were examined using scanning electron microscopy (SEM), Fourier transform infrared spectroscopy (FT-IR), differential scanning calorimetry (DSC), dynamic-mechanical thermal analysis (DMTA), tensile and impact testing.

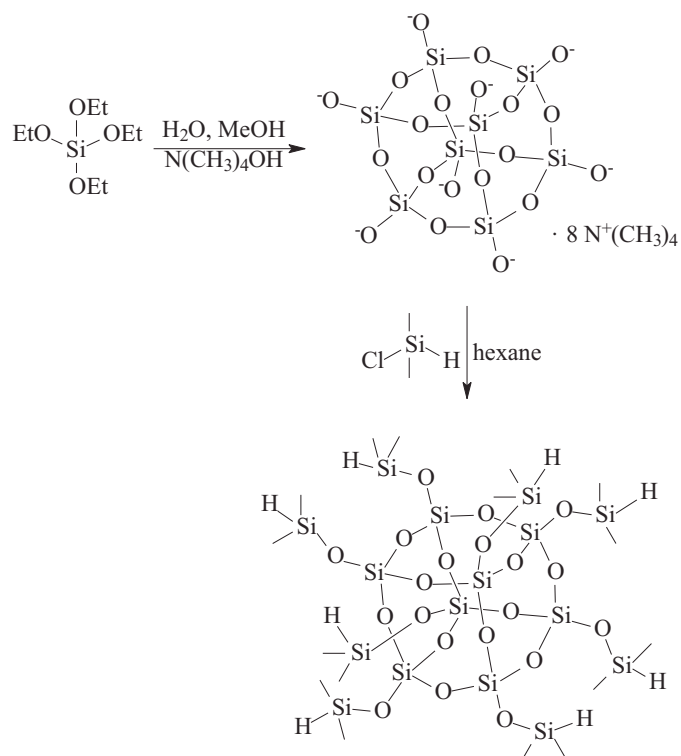
EXPERIMENTAL

Materials

Polyamide 6 (PA 6) pellets (Grade Tarnamid T27) used in this study were a product from Nitrogen Works Tarnów SA, Poland. Octakis[(3-glycidoxypropyl)dimethylsiloxy]octasilsesquioxane (POSS) was synthesized according to the two stage process published elsewhere [20]. The chemical reagents, such as tetramethylammonium hydroxide, methanol, tetraethoxysilane, petroleum ether, allyl glycidyl ether (AGE) and toluene are of chemically pure grade and were purchased from the Sigma Aldrich. Dimethylchlorosilane was purchased from the Gelest Inc. All chemicals were used as received from suppliers without any further purification.

Synthesis of octakis(dimethylsiloxy)octasilsesquioxane

Octakis(dimethylsiloxy)octasilsesquioxane was synthesized according to a procedure described by Filho *et al.* [20] (Scheme 1). In the first step 25 wt. % methanolic solution of tetramethylammonium hydroxide (164.8 mL, 1.56 mol), methanol (80 mL, 2 mol), water (60.3 mL, 3.35 mol) were placed together in 1 L flask with stirring bar. The flask was cooled in an ice bath and tetraethoxysilane (88.1 mL, 0.39 mol) was added. Solution was stirred out for 24 hours in room temperature to get octaanion solution. In the next step obtained solution was



Scheme 1. Synthesis of octakis(dimethylsiloxy)octasilsesquioxane [20]

slowly added via additional funnel to the mixture of dimethylchlorosilane (171.7 mL, 1.6 mol) and 1000 mL of petroleum ether in 2 L flask with stirrer placed in the ice bath. After whole octaanion solution was dropped, the mixture was kept in room temperature with stirring for three more hours. Next organic layer was collected and evaporated under vacuum. Obtained white powder was washed a few times with methanol and dried under vacuum to give 46 g (91 % yield) of product such as octakis(dimethylsiloxy)octasilsesquioxane.

NMR and Fourier transform infrared spectroscopy (FT-IR) analysis were employed to characterize the chemical structure of POSS. ^1H NMR (300 MHz), ^{13}C NMR (75 MHz) and ^{29}Si NMR (59 MHz) spectra were recorded on a Varian XL 300 spectrometer at room temperature using CDCl_3 as a solvent. FT-IR spectra were recorded on a Bruker Tensor 27 Fourier transform spectrometer equipped with a SPECAC Golden Gate diamond ATR unit. In all cases 16 scans at a resolution of 2 cm^{-1} were collected for spectrum. Results of FT-IR and NMR analysis confirm the structure of octakis(dimethylsiloxy)octasilsesquioxane.

FT-IR [cm^{-1}]: ν 2965 (CH); ν 2141 (SiH); ν 1254 (SiCH_3); 1070 (SiO).

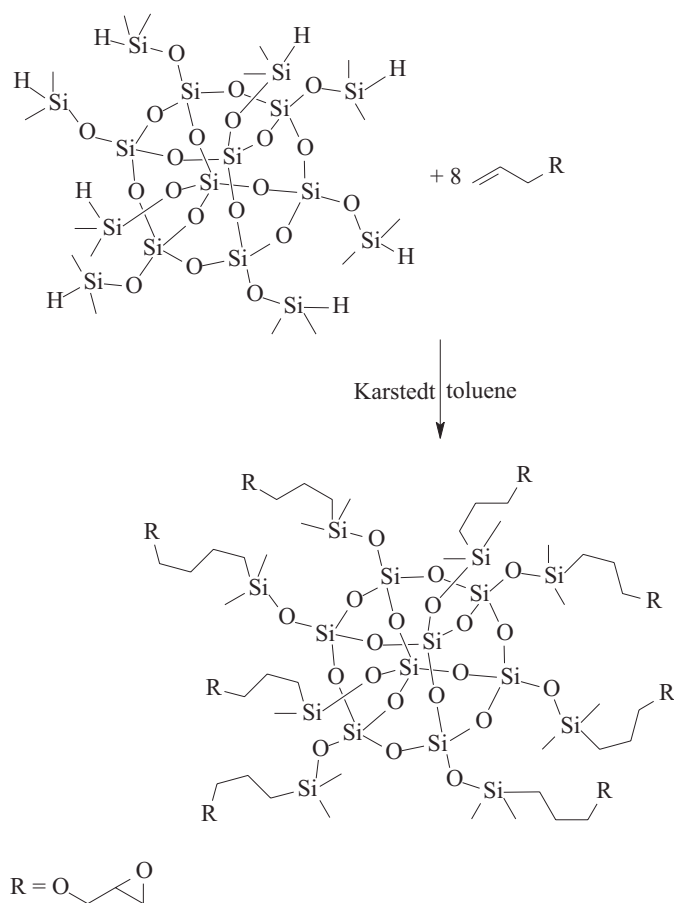
^1H NMR (CDCl_3 , 298 K, 300 MHz) δ = 0.25 (d, 48H, SiCH_3); 4.73 (m, 8H, SiH) ppm.

^{13}C NMR (CDCl_3 , 298 K, 75.5 MHz) δ = 0.037 (SiCH_3) ppm.

^{29}Si NMR (CDCl_3 , 298 K, 59.6 MHz) δ = -1.014 (HSiCH_3); -108.28 (SiOSi) ppm.

Synthesis of octakis(dimethylsiloxy, 3-glycidoxypropyl)octasilsesquioxane

Octakis(dimethylsiloxy, 3-glycidoxypropyl)octasilsesquioxane was synthesized in the hydrosilylation reaction of allyl glycidyl ether (AGE) with hydrogen silsesquioxane (Scheme 2). Process was carried out in the presence of Karstedt catalyst and toluene as a solvent.



Scheme 2. Synthesis of octakis(dimethylsiloxy, 3-glycidoxypropyl)octasilsesquioxanes [20]. Results of NMR analysis of the product confirm its structure

Octakis(dimethylsiloxy)octasilsesquioxane (5 g, 4.9 mmol), allyl glycidyl ether with 20 % excess (5.6 mL, 47 mmol) together with 50 mL of toluene as solvent were placed in three neck, round bottom flask equipped with thermometer, condenser and magnetic bar. Next Karstedt catalyst (21.4 mg, 2.35×10^{-6} mol Pt) was added in the room temperature and a solution was heated to 110 °C and kept in this temperature for 8 hours. After the reaction mixture cooled down solvent and excess of olefin were evaporated under vacuum to give the product as viscous oil (9.2 g, 97 % of theoretical).

FT-IR [cm^{-1}]: ν (CH) 3053, 2930, 2868; ν (C–O bond of epoxy groups) 1255; ν (Si–O) 1070; δ (C– bond of) 841; (epoxy groups) 910.

^1H NMR (CDCl_3 , 298 K, 300 MHz) ppm: 0.047 (OSiCH₃); 0.51 (SiCH₂); 1.51 (CH₂); 2.47, 2.65 (CH₂O); 3.00 (CHO); 3.25 (CH₂O); 3.33, 3.56 (OCH₂).

Preparation of nanocomposites

Nanocomposites containing 0.5, 2 and 4 wt. % POSS nanoparticles were prepared by melt blending in a Brabender (PLASTI-CORDER) intermeshing, twin screw extruder ($D = 42$ mm, $L/D = 6$) according to the process published elsewhere [21]. Compounding was carried out at a barrel temperature of 230 °C and a screw speed of 60 rpm. Prior to each melt processing step, all polyamide containing materials were accurately dried at 85 °C under vacuum for a minimum of 12 h.

The neat polyamide and the composites were compression molded (using frame mould) in a press at 230 °C into a plaque of 1 mm and 4 mm thickness for tensile and impact testing, respectively. The molding process was carried out using a preheating time of 8 min, pressure was applied for 5 min, and mould was immediately transferred to a cold press with applied pressure for cooling in 5 min.

Characterization

Scanning electron microscopy (SEM) observations of the surfaces, produced by fracturing of the samples cooled at liquid nitrogen and coated with gold, were made using Jeol JSM-6100 microscope.

Fourier transform infrared spectrometer (FT-IR) (Bruker Tensor 27) equipped with a SPECAC Golden Gate diamond ATR unit was used to study the chemical structure and the crystalline behavior of the nanocomposites. The samples of nanocomposites were pressed into small flakes. The specimens were sufficiently thin to be within the range of the Beer-Lambert law. In all cases 16 scans at a resolution of 2 cm^{-1} were collected for spectrum.

A Perkin Elmer differential scanning calorimeter (DSC-7) was used for thermal analysis. All experiments were run at the heating rate of 10 °C/min under a nitrogen atmosphere.

The torsion method was used with a frequency of 1 Hz, a strain level of 0.1 % in the temperature range of –150 to 100 °C. The heating rate was 3 °C/min. The testing was performed using rectangular bars measuring approximately 38 mm × 10 mm × 2 mm. These were prepared by compression molding, at a temperature of 190 °C and pressure of 100 bar, for a time period of 5 min. The exact dimensions of each sample were measured before the scan.

An Instron Series 4505 tensile tester, which operated at a crosshead speed of 50 mm/min and at room temperature was used to measure the tensile properties of the composites according to ISO 527. For each material a

minimum of 10 samples were tested to determine the average values. Prior to tests, the specimens were dried for 12 h at 85 °C in vacuum till equilibrium in moisture content (0.2 wt. %)

Notched Charpy impact tests were carried out in accordance with ISO 179 at room temperature.

RESULTS AND DISCUSSION

Microstructure of the nanocomposites

In order to explain the behavior of the nanocomposites studied in this work, the surface of fractured specimens after compression molding was examined with SEM. Figure 1 shows the morphologies of the polyamide 6/POSS composites. The dispersed particles are attri-

buted to the POSS phases. The PA 6/POSS nanocomposites showed a uniform dispersion of POSS. It seems that the reaction between epoxy functional groups of POSS and amine functional groups of polyamide 6 during melt compounding leads to *in-situ* formation of excellent dispersed POSS nanoparticles with good interfacial adhesion. However, agglomerates in the nanocomposites can be expected due to the POSS-POSS self-assembly [1].

Crystallization behavior of the nanocomposites

The FT-IR spectra of POSS, PA 6 and PA 6/POSS (96/4) nanocomposite are shown in Fig. 2. In the spectrum of POSS there is one strong band at 1070 cm^{-1} attributed to the Si–O groups and three peaks with a maximum at 1255 , 841 and 910 cm^{-1} that belong to the C–O and Si–C

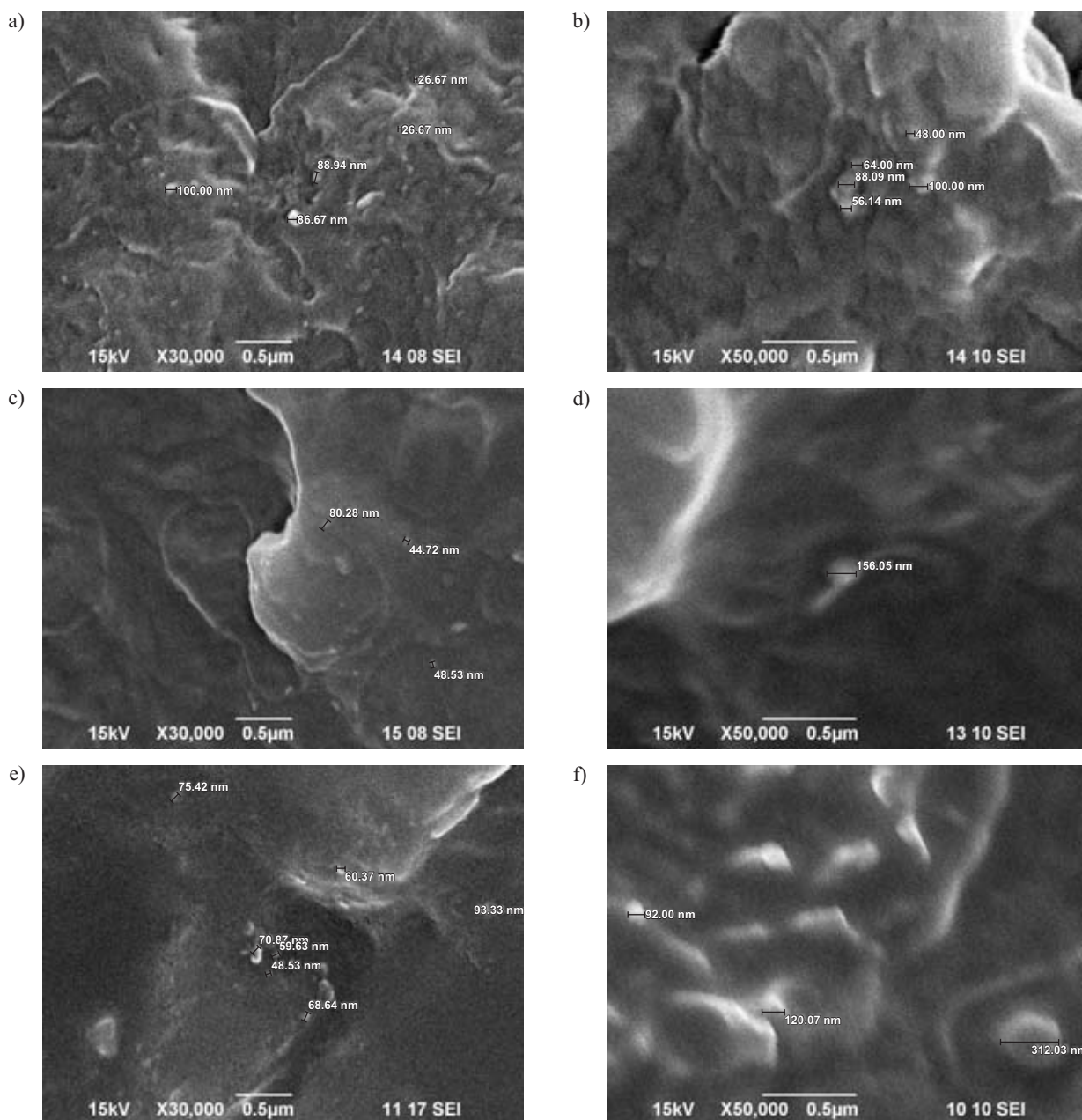


Fig. 1. SEM micrographs of PA 6/POSS nanocomposites: (a, b) 0.5 wt. % POSS, (c, d) 2 wt. % POSS, and (e, f) 4 wt. % POSS

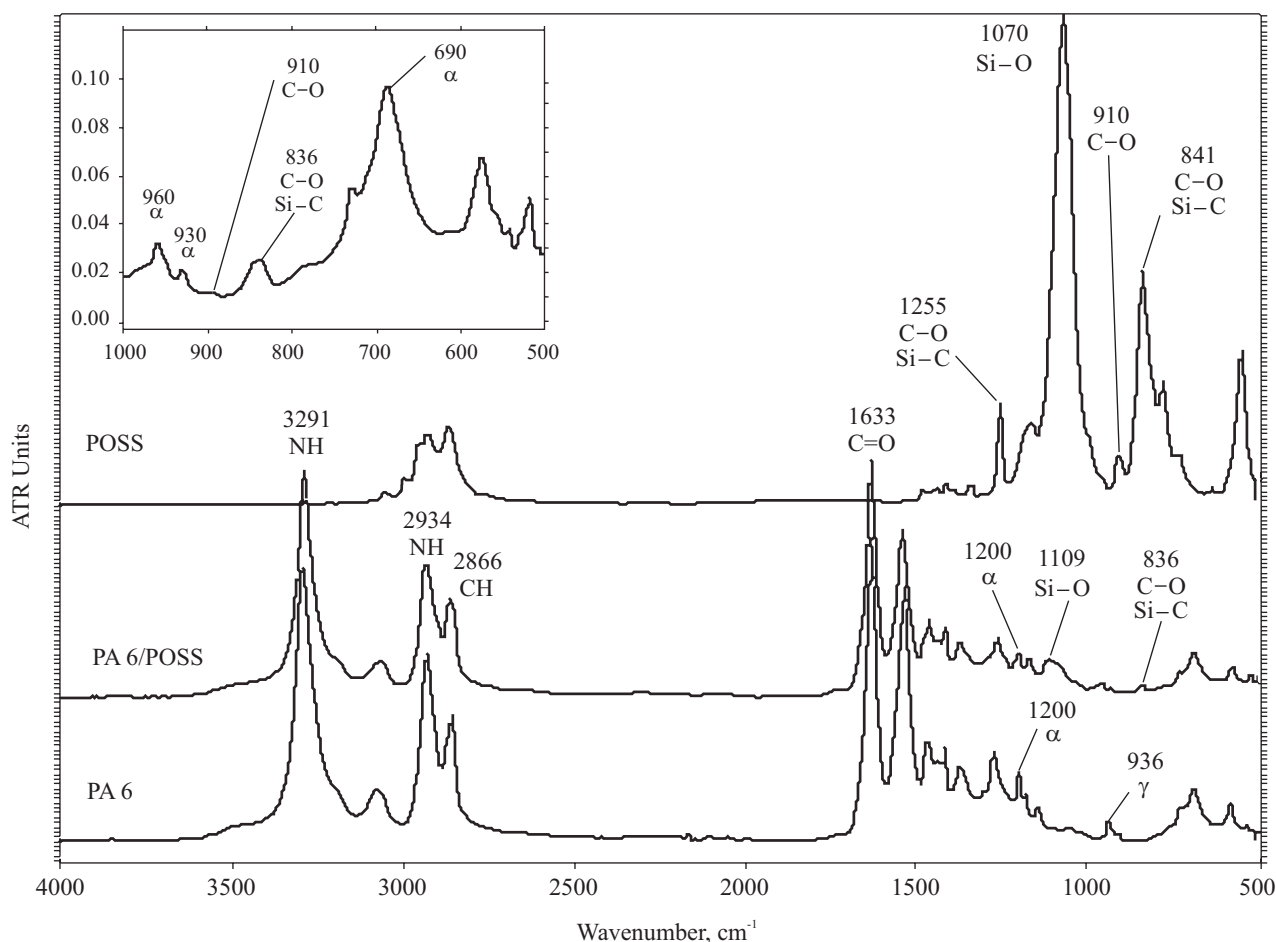


Fig. 2. FT-IR spectra of POSS, PA 6 and PA 6/POSS (96/4) nanocomposite

bonds of methyl, ether and epoxy groups and to the epoxy groups, respectively. In the spectrum of PA 6/POSS (94/6) nanocomposite, the absorbance of Si–O groups of POSS is moved to a higher wave number compared with the POSS, suggesting that functional groups of POSS could be selectively bonded with functional groups of PA 6. The absorption peak at 841 cm^{-1} corresponding to the epoxy groups was moved to the lower wave number, probably as a result of the interactions that took place between the epoxy groups of POSS and the amine groups of PA 6. The lower intensity of the peaks of epoxy groups in the PA 6/POSS nanocomposite is further proof that most of the epoxy groups of POSS react with the amine groups of PA 6.

The existence of an absorption peak at 690 and 1200 cm^{-1} indicates that both PA 6 and PA 6/POSS nanocomposites are in α crystalline form. It is noted that the new absorption peaks at 930 and 960 cm^{-1} appeared in the PA 6/POSS spectrum, which confirms α crystalline form of the PA 6. Moreover, in the spectrum of PA 6 there is a small band at 936 cm^{-1} , which probably corresponds to γ phase crystals of the PA 6. Thus, the addition of POSS affects the crystallinity of the polyamide.

In order to obtain more information regarding the crystallization behavior of the samples, DSC was used. Figure 3 shows the second heating and cooling DSC

curves of PA 6 and PA 6 with different amount of POSS. The DSC data presented in Table 1 show that the glass transition temperature (T_g) and crystallization temperature (T_c) were shifted significantly to a higher temperature for PA 6/POSS composites. The addition of POSS raised the glass transition temperature by 28 °C. The crystallization temperature increased from 163 to 189 °C, indicating that POSS acts as heterogeneous crystallization nucleator of the matrix and increases the crystallization rate of PA 6 and the degree of crystallinity (X_c) of PA 6. On the other hand, POSS also acts as a physical hindrance which retards the crystallization of PA 6 molecular chains

Table 1. Glass transition and crystallization parameters of PA 6 and PA 6/POSS nanocomposites measured by DSC

POSS content wt. %	T_g , °C	T_m , °C	T_c , °C	X_c^* , %
0	28	218	163	40.1
0.5	53	215, 222	188	43.2
2	53	215, 222	189	43.0
4	53	215, 221	189	45.7

* Assessed by integrating the normalized area of the melting endothermic peak and rationing the heat involved to the reference value of 100 % crystalline PA 6 (190 J/g).

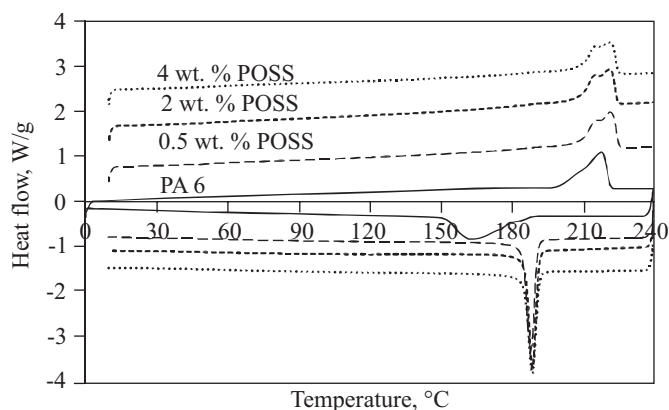


Fig. 3. DSC curves of PA 6/POSS nanocomposites with different fractions of POSS

for the physical and chemical interactions. The combination of these two factors makes the PA 6 chains arrange orderly at a higher temperature, which results in the increase of T_c .

The crystalline structures of PA 6 are related to many factors, such as thermal treatment, stress history and the presence of moisture, additives and nanofillers. In general, the α form is thermodynamically stable, but the γ form is kinetically favored, and they are usually associated with two different melting temperatures, 221 and 215 °C, respectively [12, 22].

From DSC curves (Fig. 3), it can be seen that the PA 6 has only one melting peak at 218 °C, which is associated with melting of the less stable γ form crystals of PA 6 [23]. This indicates that in neat PA 6 the γ crystal is the dominant crystalline phase. Moreover, in the PA 6 a shoulder prior to the endothermic peak could be clearly observed. In contrast, two melting peaks appear in the curves of PA 6/POSS composites. Next to the melting peak at 222 °C, the addition of POSS into the polymer matrix induces a lower endothermic peak (T_m , γ) at 215 °C as a shoulder of T_m , α , which may be related to the melting of the less stable γ form crystals of PA 6 [23], or it may simply reflect changes in crystalline thickness and distribution of the α form [12]. Thus, the existence of POSS affects the crystallinity of the polyamide.

Tensile and impact properties

The tensile properties of PA 6 and PA 6/POSS composites are given in Table 2. Typical stress-strain curves of the various investigated composites, shown in Fig. 4, indicate that the mechanical behavior of POSS modified polyamide was considerably different from that of neat PA 6. It is interesting to note, that used polyamide 6 shows extremely small elongation at break and low impact strength. This phenomenon may be caused by the thermal treatment, stress history, the presence of moisture and the method of specimens molding. In general, the dried samples of PA 6 exhibit much lower elongation and impact strength in comparison with the ones condi-

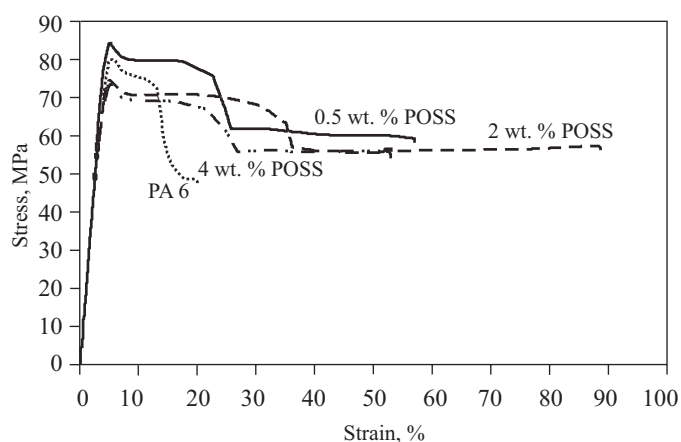


Fig. 4. Stress-strain curves of PA 6/POSS nanocomposites with different fractions of POSS

tioned once. Also the compression molded specimens have poorer mechanical properties than injection molded. Comparing all composites, the addition of POSS causes a substantial increase of 10–20 % in tensile strength at break in comparison to the initial value. The maximum value was observed for low POSS loading at 0.5 wt. %. On the other hand, the addition of POSS does have a significant effect on tensile strength. Theoretically, the tensile strength of the composites is usually lower than that of the unfilled polymer due to the particles are unable to bear any fraction of the external load during tensile loading. However, opposite results has been shown in Fig. 4. In fact, the increase in tensile strength is observed at 0.5 wt. % filler content. The enhancement in tensile strength could indicate that the bonding between POSS and matrix is strong enough and the particle could withstand the external load applied during tensile loading. For POSS concentrations higher than 0.5 wt. % a small decrease about 5 % is observed. This behavior could be attributed to tendency of POSS to form agglomerates at higher concentrations, as already proved by SEM study. This is in agreement with a similar deterioration of mechanical properties reported for PA 6/spherical silica nanocomposites [24].

Table 2. Mechanical properties of PA 6 and PA 6/POSS nanocomposites (dried samples)

POSS content wt. %	Tensile strength MPa	Tensile strength at break MPa	Elongation at break, %	Charpy notched impact strength kJ/m ²
0	79.8 ± 2.0	48.9 ± 6.7	22 ± 6	2.7 ± 2.1
0.5	84.8 ± 3.6	62.6 ± 4.2	59 ± 5	9.2 ± 0.5
2	75.3 ± 1.6	56.5 ± 3.6	90 ± 10	9.7 ± 0.4
4	74.9 ± 1.2	55.6 ± 5.1	54 ± 7	5.6 ± 0.3

The addition of POSS has a positive effect on the elongation at break. A gradual increase in elongation at break

is observed for POSS contents up to 2 wt. %, reaching 414 % in comparison to the initial value. For POSS concentration higher than 2 wt. % a significant decrease is observed due to the POSS-POSS self-assembly. However, the value is over 150 % higher in comparison with neat polyamide 6. This improvement in elongation for composites should be associated with small agglomerations of POSS nanoparticles, which could act as stress concentrators of failure points of the material. It seems that epoxy functional groups in POSS result in uniform dispersion of the nanoparticles and good adhesion between them and the matrix. Therefore, the interaction between the particles and the matrix is considerable, making it easier for properties to be transferred between the two materials.

Moreover, a gradual increase of 87–223 % in notched Charpy impact strength is achieved in the PA 6/POSS nanocomposites. The maximum was observed at POSS loading of 2 wt. %. The decrease in impact strength at higher POSS content can be explained due to the possible aggregation of POSS nanoparticles at higher concentrations. However, the results suggest that POSS is effective in improving the impact strength of the composites.

The above mentioned results show that the properties of the nanocomposites formed by melt compounding are highly dependent upon the POSS contents. The increase in mechanical properties is mainly due to the uniform dispersion of POSS in the composites and good adhesion between them and the matrix. It is also likely that POSS nanoparticles orientation as well as molecular orientation contribute to the observed reinforcement effects.

Dynamic-Mechanical Properties

Dynamic-mechanical thermal analysis (DMTA) can provide reliable information about the relaxation behavior of the examined materials. In order to evaluate the effect of POSS nanoparticles on the PA 6 matrix, thermo-mechanical properties were measured. Due to the very high surface area and epoxy functional groups of the nanoparticles in the PA 6/POSS nanocomposites, the applied stresses are expected to be easily transferred from the matrix onto the POSS particles, resulting in an enhancement of the mechanical properties. The epoxy functional groups of POSS can react with amine functional groups of polyamide 6 and break up the large agglomerates of the nanoparticles into finer particles, resulting in an increase in their degree of dispersion in the polymeric matrix, increasing the interfacial adhesion.

Figure 5a shows the dynamic storage modulus (G') versus temperature of various PA 6/POSS nanocomposites. From Figure 5a, it can be seen that the addition of POSS significantly increases G' of PA 6, especially below the glass transition temperature, which is due to the stiffening effect of the POSS. As seen in Table 3, the G' of polyamide 6 at 25 °C is improved by about 75–88 %. POSS could affect the PA 6 chain through the active centres

Table 3. DMTA results for PA 6 and the PA 6/POSS nanocomposites

POSS wt. %	Storage modulus, Pa	Loss tangent (peak position), °C		
	at 25 °C	T_γ	T_β	T_α
0	$0.88 \cdot 10^9$	-148.1	-73.3	25.5
0.5	$1.54 \cdot 10^9$	-139.5	-70.2	54.9
2	$1.65 \cdot 10^9$	-139.0	-65.7	56.7
4	$1.61 \cdot 10^9$	-143.3	-66.1	57.2

formed by silanol or epoxy functional groups and through the reaction with amine functional groups of PA 6 and hinder the chain motion of PA 6, which would improve the modulus. As a result of these changes, the storage modulus of the interface is higher than that of the free part. An increase in the POSS content enlarges the interfacial area and results in increased volume of interphase. However, at higher POSS content (4 wt. %) the particles tend to form extended agglomerates (see SEM micrographs of Fig. 1e, f) and as a result the interphase is re-

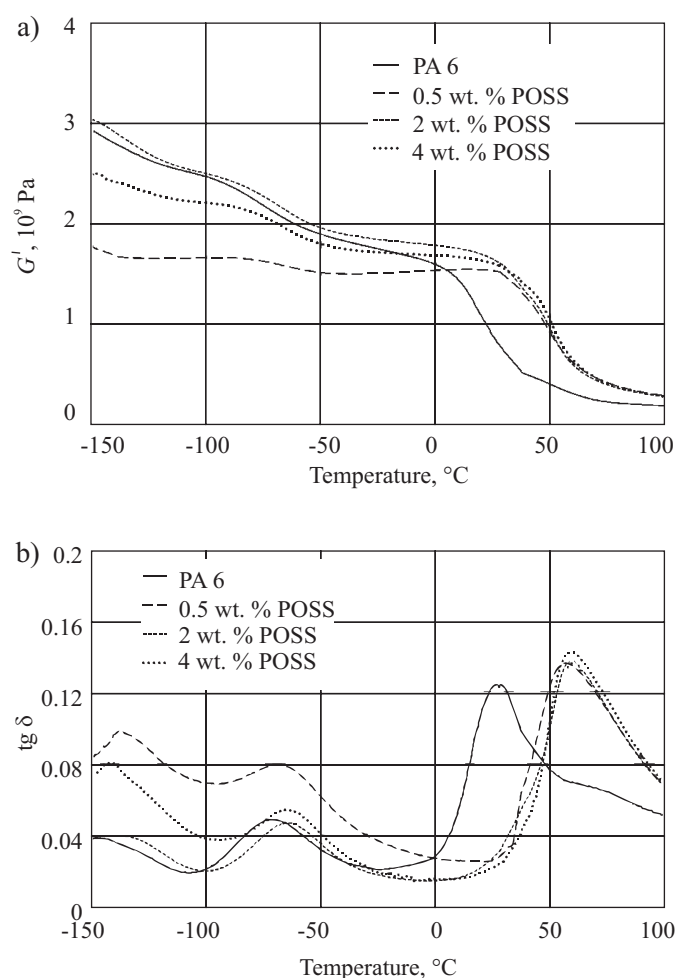


Fig. 5. Dynamic mechanical relaxation behavior versus temperature of PA 6 and PA 6/POSS nanocomposites at frequency of 1 Hz: (a) G' , (b) $\tan \delta$

duced. Therefore, above the glass transition temperature, the storage modulus of PA 6/POSS composite containing 4 wt. % POSS is lower than the one containing 2 wt. % POSS.

Figure 5b presents the temperature dependence of the loss tangent ($\tan \delta$) of PA 6 and PA 6/POSS nanocomposites. The $\tan \delta$ maximums show three (α , β and γ) relaxations, which take place in the specimens in order of decreasing temperature, respectively. These are accompanied by a pronounced decrease of the storage modulus.

The α -relaxation corresponds to the glass transition temperature (T_g), as shown in Fig. 5b. The glass transition temperature increases from 25 °C for the neat PA 6 to 55–57 °C for PA 6/POSS nanocomposites (Tab. 3). It is well known that in polymer matrix composites, the T_g on the polymer matrix depends on the free volume of the polymer, which is related to the affinity between the filler and the polymer matrix [25, 26].

The β -relaxation can be observed as a clear maximum, which temperature increases as a function of POSS content (Fig. 5b and Tab. 3). It was reported that the β -relaxation results from motions of amide polar groups in the interfacial region and is attributed to the glass transition [27].

The γ -relaxation has been associated with a single relaxation process, predominantly of amorphous origin. The γ -relaxation appears as a maximum at about –148 °C for the PA 6 and in the range from –143 to –139 °C for the nanocomposites (Fig. 5b, Tab. 3), with a corresponding decrease in storage modulus (Fig. 5a). This is a clear effect of POSS content on the breadth and on the location of the relaxation; this process is shifted toward higher temperature in the presence of POSS, as a consequence of higher crystallinity.

CONCLUSIONS

The morphology, thermal and mechanical properties of PA 6/POSS composites have been investigated. SEM results showed that POSS are uniformly dispersed in polyamide 6 matrix. FT-IR and DSC analysis indicated that the addition of POSS promotes modifications of the polyamide crystal structure, which consist of the progressive development of α crystals and significant increase in the glass transition temperature, crystallization temperature and the crystallization rate of the polyamide 6. Mechanical testing, carried out above the material's glass-transition temperature, showed that the presence of POSS resulted in increased strength and significantly improved elongation at break relative to that in the neat PA 6. Moreover, the addition of POSS improved impact strength of polyamide 6. Dynamic mechanical thermal analysis showed that the addition of POSS significantly increased the G' and relaxation temperatures (T_{α} , T_{β} and T_{γ}), especially glass transition temperature (T_g) of PA 6, due to the greatly limited molecular motion. These effects can be mainly attributed to the chemical bonding between the epoxy groups of POSS and amine groups of PA 6, the

increase in the degree of crystallinity and also to the development of α form, which was promoted by POSS modification.

ACKNOWLEDGMENTS

This research was supported by Ministry of Science and Higher Education grant No 05-0005-04/2008. The authors are grateful to Dr. Aneta Łukomska and MSc. Maciej Studziński from Industrial Chemistry Research Institute for providing the SEM microphotographs and DMTA analysis, respectively.

REFERENCES

- Liu L., Tian M., Zhang W., Zhang L., Mark J. E.: *Polymer* 2007, **48**, 3201.
- Marciniak B.: *Przem. Chem.* 2010, **89**, 1184.
- Joshi M., Butola B. S.: *Polymer* 2004, **45**, 4953.
- Li B., Zhang Y., Wang S., Ji J.: *Eur. Polym. J.* 2009, **45**, 2202.
- Dasari A., Yu Z. Z., Mai Y. W., Cai G., Song H.: *Polymer* 2009, **50**, 1577.
- Zhao F., Bao X., McLauchlin A. R., Gu J., Wan C., Kandasubramanian B.: *Appl. Clay Sci.* 2010, **47**, 249.
- Kim H., Bang Y. H., Choi S. M., Yoon K. H.: *Compos. Sci. Technol.* 2008, **68**, 2739.
- Li G. Z., Wang L., Toghiani H., Daulton T. L., Koyama K., Pittman C. U.: *Macromolecules* 2001, **34**, 8686.
- Dias M. L., Fernandes M. J. A.: *Polym. Eng. Sci.* 2000, **40**, 2482.
- Ma J., Qi Z., Hu Y.: *J. Appl. Polym. Sci.* 2001, **82**, 3611.
- Fornes T. D., Yoon P. J., Keskkula H., Paul D. R.: *Polymer* 2001, **42**, 9929.
- Fornes T. D., Paul D. R.: *Polymer* 2003, **44**, 3945.
- Gołębiewski J., Róžański A., Gałęski A.: *Polimery* 2006, **51**, 374.
- Piłatowski J., Kiersznowski A., Dołęga J.: *Polimery* 2006, **51**, 704.
- Kelar K., Jurkowski B., Mencil A.: *Polimery* 2005, **50**, 449.
- Cho J. W., Paul D. R.: *Polymer* 2001, **42**, 1083.
- Rong M. Z., Zhang M. Q., Ruan W. H.: *Mater. Sci. Technol.* 2006, **22**, 787.
- Jeziórska R., Klepka T., Paukszta D.: *Polimery* 2007, **52**, 294.
- Fina A., Tabuani D., Fracht A., Camino G.: *Polymer* 2005, **46**, 7855.
- Filho N. L. D., de Aquino H. A., Pires G., Caetano L.: *J. Braz. Chem. Soc.* 2006, **17**, 533.
- Polish Patent Application P-393093 (2010).
- Bureau M. N., Denault J., Cole K. C., Enright G. D.: *Polym. Eng. Sci.* 2002, **42**, 1897.
- Liu L. M., Qi Z. N., Zhu X. G.: *J. Appl. Polym. Sci.* 1999, **71**, 1133.
- Jeziórska R., Zielecka M., Świerz-Motysia B., Studziński M.: *Polimery* 2009, **54**, 727.
- Yuen S. M., Ma C.-C. M., Lin Y.-Y., Kuan H.-C.: *Compos. Sci. Technol.* 2007, **67**, 2564.
- Menard K. P.: "Dynamic mechanical analysis", CRC Press, Florida, 1999.
- Ray S. S., Okamoto M.: *Prog. Polym. Sci.* 2003, **28**, 1539.

Received 5 I 2011.